Design-oriented Finite Element Study of a 3D Printed Acrylonitrile Styrene Acrylate Pressure Enclosure Using Effective Material Properties

Arman Heydari
Instituto de Investigación para la Gestión Integrada de Zonas Costeras
Universitat Politècnica de València
València, Spain
Aheydar@upv.edu.es

Jaime Lloret
Instituto de Investigación para la Gestión Integrada de Zonas Costeras
Universitat Politècnica de València
València, Spain
jlloret@dcom.upv.es

Abstract - The mechanical response of a 3D-printed Acrylonitrile Styrene Acrylate (ASA) container under uniform external pressure is examined in this study. The container is produced using additive manufacturing, where the presence of infill plays an important role in the overall behavior. For this reason, the effect of infill is not ignored. Instead, effective material properties are estimated using a Representative Volume Element (RVE) model and later applied in the finite element analysis of the full container. The numerical simulations correspond to external pressures associated with depths of 50, 70, and 100 m. At each depth, the stress distribution and displacement of the structure are evaluated. The results do not show any sudden changes in behavior within this range. Both stress and deformation increase with pressure, and the response remains essentially linear elastic. When the results obtained for the solid material are compared with those including infill-based properties, differences in deformation become evident. The maximum stress values, however, remain very similar. This observation suggests that infill mainly affects stiffness rather than stress level. From a practical point of view, the container can be considered safe up to 100 m in depth when compared with the reported yield stress of ASA. The approach used in this work may therefore be helpful during the early stages of design.

Keywords - Additive manufacturing; ASA; homogenization; infill; finite element analysis; pressure loading.

I. INTRODUCTION

In recent years, additive manufacturing, and in particular polymer 3D printing, has received widespread attention as an alternative technology to produce engineering parts with complex geometries. The ability to produce quickly, reduce manufacturing costs, and minimize material waste are among the factors that make this technology attractive for Performance oriented engineering applications. Among these applications, the design and manufacture of enclosures and bodies subjected to external pressure, particularly in underwater systems, have been proposed as emerging areas. Enclosures used in underwater environments usually must meet other requirements such as low weight, economical manufacturing, and the possibility of implementing complex geometries in addition to withstanding hydrostatic pressure. In this regard, polymer 3D printing can be a suitable alternative to traditional manufacturing methods.

Existing real-world deployments of underwater and distributed sensing systems further emphasize the need for reliable and mechanically robust enclosures in operational environments [1]. Additively manufactured enclosures can be relevant in practical underwater systems, where compact and lightweight housings are required for the integration of sensing and electronic components [2]. However, the mechanical behavior of printed parts under external pressure requires careful, informed investigation, given the inherent characteristics of additive manufacturing. One of the most critical challenges in the numerical analysis of 3D-printed parts is accounting for the internal infill structure. Infill, which is used to reduce weight and manufacturing time, leads to the creation of a heterogeneous microstructure inside the part and, as a result, changes the effective mechanical properties of the material compared to the bulk state. Ignoring this issue can lead to inaccurate estimates of the structure's stiffness and deformation behavior, particularly in applications where deformation limits are critical. In many existing numerical studies, the effect of infill is either completely ignored or accounted for using empirical reduction factors applied to material properties. Although these approaches are helpful for simple initial estimates, their strong dependence on the type of infill, print pattern, and manufacturing conditions limits the generalizability of the results. On the other hand, explicit modeling of the infill geometry at the structural scale is not practical and cost-effective for design-oriented analyses due to its geometric complexity and high computational cost.

Accordingly, the use of homogenization and multiscale approaches is proposed as a suitable approach to account for the infill effect without increasing the complexity of the structural model. In this study, a design-oriented numerical framework is presented to investigate the mechanical behavior of a 3D printed ASA container under uniform external pressure. First, the material's effective mechanical properties are extracted using a volumetric representative model, and these properties are subsequently incorporated into the finite element analysis of the container. The structural behavior of the container is investigated under equivalent pressures at different depths, and the results are discussed in terms of stress, deformation, and safety margin relative to the material's yield stress.

The remainder of the paper is structured as follows. Section 2 reviews the related works and provides background on underwater enclosures and the mechanical behavior of additively manufactured parts. Section 3 presents the proposed methodology, including the design considerations, material selection, geometrical configuration of the enclosure, effective material modeling based on the infill structure, and the finite element framework used for the

structural analysis. Section 4 reports the numerical results obtained under different external pressure levels, while Section 5 discusses these results in terms of structural performance, stress distribution, and deformation behavior. Finally, Section 6 concludes the paper and highlights the main findings and potential directions for future work.

II. Related Work

Nowadays, deployments of underwater and aquatic monitoring systems and wireless sensor networks are significantly increasing, as these technologies are being used in a wide range of scientific, environmental, and industrial applications. This growing reliance on sensing units operating in submerged and often harsh conditions simultaneously raises the need for reliable, isolated, and mechanically robust housings to ensure their continuous and stable performance. In such environments, protective enclosures play a key role in maintaining device integrity, preventing damage from external pressure and environmental influences, and ultimately supporting the long-term functionality of underwater sensing systems [1][2].

Fused Filament Fabrication (FFF) 3D printing is widely used to fabricate polymer parts, mainly because the fabrication process is simple and does not require complex equipment. However, it is obvious that the parts produced by this method cannot be considered as completely uniform materials due to the way the parts are fabricated. For example, studies have shown that by changing the printing direction, significant changes in the stiffness and strength of the parts can be achieved. Ahn et al. were among the first to demonstrate this experimentally and directly relate it to the layer-by-layer printing process [3]. Similar behavior has also been reported for various thermoplastic polymers, and it has been shown that the internal arrangement formed during printing plays a decisive role in the load transfer within the part [4][5].

ASA has been increasingly considered for FFF applications, especially where better environmental resistance than ABS is required. Cahyadi reported stress-strain curves and Young's modulus values by performing tensile tests on printed ASA samples and showed that these properties are strongly dependent on the printing parameters [6]. In a different approach, Yap et al. investigated the mechanical response of ASA parts by combining ultrasonic measurements and finite element analysis [7]. Their results showed that the properties extracted from the tests can be used in numerical simulations, although the material behavior remains dependent on the printing direction. Hameed et al. also investigated the effect of process parameters on the elastic modulus and tensile strength of ASA using the Taguchi design of experiments and reported a similar trend [8].

Instead of focusing on ASA, some studies have investigated the behavior of this polymer in comparison with other common polymers in FFF. Vázquez-Martínez et al. showed that different printing strategies can have a significant impact on the mechanical behavior and wear of ASA parts [9]. Their results indicate that even relatively small changes in the internal structure can lead to significant differences in the final part performance. This suggests that material selection alone is not sufficient to achieve the desired performance and that the internal structure of the part should also be considered as part of the design process. The effect of infill, or the percentage of filling between the printed walls of the part, on the mechanical behavior of printed parts has been investigated in several experimental studies. In general, increasing the infill density leads to an increase in the stiffness and strength of the part, although this relationship is not necessarily completely linear [10], [11]. By combining mechanical tests and finite element simulations, Rankouhi et al. showed that numerical predictions of the behavior of printed parts are only reliable if the effect of the internal structure is included in the model [12]. Similar results have been reported in failure studies, where neglecting the infill has led to incorrect calculations of critical stresses and damage parameters [13].

In terms of numerical modeling, two main strategies are commonly used to consider the effect of the infill. In one approach, the infill geometry is explicitly modeled in a finite element mesh, which, although allows for a detailed investigation of the local stress distribution, has a high computational cost [12]. In the second approach, the internal structure is derived using effective material properties and is replaced by homogenization methods [14][15]. These methods are often based on classical concepts of cellular materials, such as the framework presented by Gibson and Ashby, and allow for the effect of the internal structure to be considered without excessively increasing the complexity of the model [14].

Despite the large body of studies on the mechanical behavior of FFF parts and the role of infill, most of these studies have focused on tensile or bending loading. Investigations of polymer structures under external pressure, which is important for applications such as pressure vessels, have been much less reported [16][17]. Furthermore, the use of effective properties due to infill in the framework of a design-oriented finite element analysis for ASA parts has not been widely investigated. The present study aims to address this gap by numerically analyzing an ASA vessel under external pressure using effective material properties. Overall, this study contributes by addressing the limited investigation of FFF structures under external pressure and by incorporating effective material properties into a practical design-oriented numerical framework.

III. METHODOLOGY

A. Design Considerations and Material Selection

This section describes the main design considerations and material selection criteria adopted in the development of the 3D-printed enclosure. The functional requirements, operating conditions, and practical constraints of underwater applications are taken into account in defining the overall design approach. In addition, the rationale behind selecting the printing material and manufacturing strategy is discussed, providing the basis for the subsequent numerical analysis. The design problem was to develop a housing to carry a set of sensors and electronic equipment in the underwater marine environment. This housing consists of two separate sections: one section for housing the electronic boards and sensors, and the other section for carrying the battery. Due to the variety of sensors and the complexity of the internal component arrangement, the final geometry of the housing was inherently complex.

To control manufacturing costs, reduce production time, and enable rapid design modification and iteration, parts were manufactured using a 3D printer using the Fused Filament Fabrication method. As is evident, this method allows the production of complex geometries without the need for molding and is very suitable for design-oriented applications.

In selecting the material, the limitations associated with filamentary polymer materials, the limitations of the 3D printer, and the operating conditions in the underwater environment were considered. Among the available materials, ASA was selected due to its suitable mechanical properties, thermal stability, and better resistance to environmental conditions. Literature reports also show that ASA has lower water absorption than ABS, which is important for underwater applications. Therefore, the other subfamily of this group, ABS, was removed from the list of materials considered. Although there is a wider variety of polymer materials for 3D printing, many of them require more advanced equipment and specific printing operating conditions. In particular, some materials require higher temperatures at the nozzle and the printing bed, which increases the cost of the device and the complexity of the process. Given that ASA can be printed at temperatures of about 240 ° C for the nozzle and about 90-100 ° C for the printing bed, its use is possible with existing equipment and is relatively economically justified.

B. Geometrical Design and Structural Layout

Several initial ideas were considered for the design of the enclosure. In all of these designs, printing time constraints, printable dimensions with the existing machine, and resistance to high pressure were considered as the main factors. Given the need for the enclosure to operate at depths of more than 40 meters, the initial design started with geometries close to spherical structures, as these types of geometries are inherently suitable for withstanding external pressure. After examining various options, the final design resulted in a capsule structure that, while maintaining adequate resistance to external pressure, provided the most useful internal space for placing equipment and also provided greater and better access for maintenance. The thickness of the walls was chosen by considering the required internal space, the dimensional constraints of the printer, and the need to provide sufficient structural strength.

The enclosure consists of four main parts. At the junction of the sensor-carrying section and the battery-carrying section, a flange is provided for assembling these two parts. The parts are connected to each other by screws to allow assembly, disassembly and repairability. The final geometry of the enclosure and the overall assembly layout resulting from this design process are shown in Figure 1.

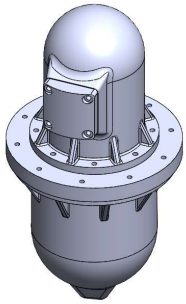

Figure 1: Geometry of the pressure enclosure and assembly layout – isometric view

C. Effective Material Modeling Based on Infill Structure

In the initial analysis phase, the enclosure was modeled as a solid using the reported mechanical properties of ASA. The Young's modulus of the material was assumed to be:

$$E = 1850 \text{ MPa} \quad (1)$$

This value was selected based on experimental studies reported in the literature. In order to investigate the overall strength of the enclosure, the reduction in printing time by using a lower percentage of infill was investigated. Hence, a homogenization approach was used to extract the effective Young's modulus. In this regard, a Representative Volume Element (RVE) model with dimensions $10 \times 10 \times 10mm^3$ created.
In this model, the infill structure was considered based on the actual printing process specifications including layer height, wall width, and extrusion width. These parameters were chosen to suit a printer equipped with a 0.4 mm nozzle. The representative volume element used to model the infill architecture and printing parameters is illustrated in Figure 2.

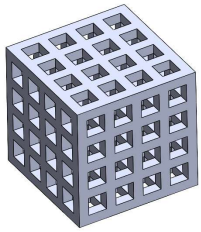

Figure 2: RVE model with infill architecture and printing parameters

To extract the effective modulus, one side of the RVE model was fully constrained, and a uniform displacement was introduced to the opposite side. Finally, the reaction force value was read. This value was equal to 1.69 MPa. This value represents the macro stress. Then the macro strain was calculated. And by dividing this value, we arrived at the effective modulus value. The effective Young's modulus is obtained as:

$$E_{\text{eff}} = \frac{\sigma_{\text{macro}}}{\varepsilon_{\text{macro}}} = \frac{1.69}{0.001} = 1690 \text{ MPa} \quad (2)$$

Comparing this value with the modulus of the material with 100% infill showed that the porosity, load transfer path, and infill architecture resulted in a reduction of about 9% in effective stiffness. With this effective modulus, there was no need to model the infill at the structural scale, and the enclosure was modeled as a homogeneous material with the new effective properties calculated.

D. Finite Element Model and Boundary Conditions

Numerical simulations were carried out in Abaqus. The geometry was discretized with 3D triangular elements, applying a maximum element size of 6 mm. In the finite element setup, bolt positions were coupled to reference points, where displacements were

fully constrained while moments were left unconstrained. This approach simplifies the bolt connection, allowing for efficient extraction of the necessary results. The finite element discretization of the enclosure and the applied boundary conditions are shown in Figures 3 and 4, respectively.

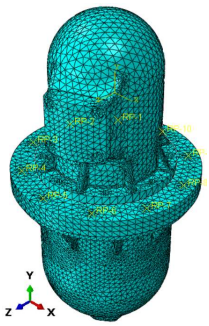

Figure 3: Finite element mesh

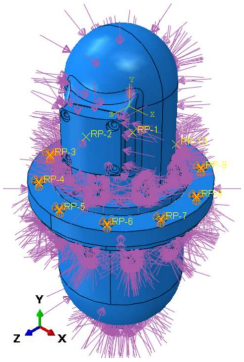

Figure 4: Finite element boundary conditions

The loading is applied as an external pressure resulting from the pressure difference between the environment and the inside of the chamber. Since the pressure inside the chamber is approximately equal to atmospheric pressure, only the pressure difference is considered in the analysis. This simplified method is modeled and is well suited for design-oriented analyses. The external pressure corresponding to a depth of 50 meters is equal to: $p = 0.5$ MPa was considered and this pressure was applied to all external surfaces in contact with seawater. Analyses were also performed for greater depths with a proportional increase in pressure.

E. Output Quantities and Evaluation Criteria

The studies were conducted at external pressures from depths of 50, 70, and 100 meters. These studies were conducted at two cases: a normal modulus of 1850 and an infill of 1690; the results are presented. In all contour plots, stresses are reported in terms of von Mises stress in MPa, while displacements are expressed in millimeters.

A representative von Mises stress distribution for an external pressure corresponding to a depth of 50 m is shown in Figure 5 and the corresponding total displacement field for the same loading condition is presented in Figure 6.

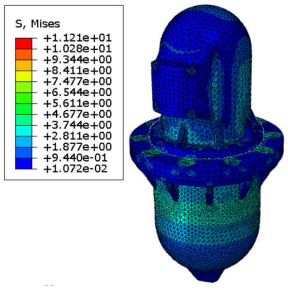

Figure 5: Von Mises stress contour at 50 meters depth

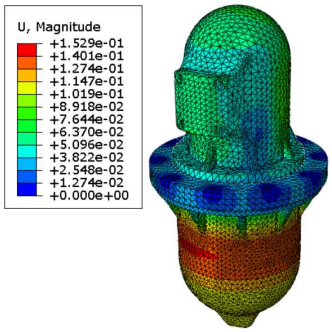

Figure 6: Displacement contour at 50 meters depths

IV. Results

In this section, we share what we observed when putting the ASA enclosure to the test under several different external pressures. We wanted to find out the maximum von Mises stress and the greatest displacement the enclosure would face at pressures matching 0.5, 0.7, and 1 MPa. For every pressure scenario, we analyzed the enclosure twice: once with solid ASA, and once with a material that incorporates the effective properties determined by the RVE analysis. By comparing these sets of results, we gained a clear picture of how the enclosure performs depending on which material model is used, while keeping the loading conditions the same.

A. Numerical Results

The numerical results obtained at different external pressures for different values of Young's modulus are summarized in Table 1. As shown, with increasing external pressure, the maximum von Mises stress and maximum displacement increase in both material models. For all investigated pressure levels, the maximum stress values in the two material models do not differ significantly from each other, while the maximum displacement in the model based on effective properties is uniformly larger than that of the bulk material.

Depth (m)	Pressure (Mpa)	Young's Modulus (Mpa)	Max Von Mises (Mpa)	Max Displacement (mm)
50	0.5	1850	11.21	0.1397
50	0.5	1690	11.21	0.1529
70	0.7	1850	15.69	0.1955
70	0.7	1690	15.69	0.214
100	1	1850	22.42	0.2793
100	1	1690	22.42	0.3058

Table I: Maximum von Mises stress and displacement under different external pressures.

B. *Effect of External Pressure*

To better understand how the structure shifts as we increase the external pressure, The variation of the maximum displacement with external pressure for both material models is shown in Figure 7. It's clear from the graph that the higher the pressure, the more the structure moves—and this increase is almost perfectly linear. When we switched to the effective properties model, which has a lower Young's modulus, we saw even greater displacement at every pressure point. Still, the general way the structure responds doesn't really change between the two materials.

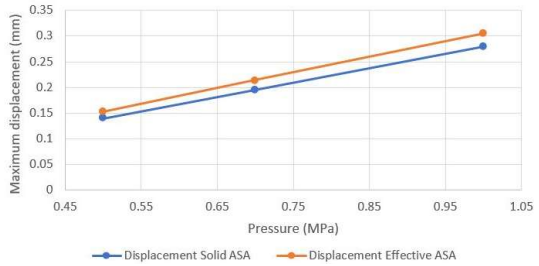

Figure 7: Maximum displacement versus external pressure for solid and effective ASA material models

C. *Qualitative Stress and Displacement Distribution*

To help you visualize how the structure responds, we focused on a typical case and examined both the von Mises stress distribution and the total displacement. Our goal was to show the main trends in stress and deformation throughout the structure, not to get bogged down in comparing precise numbers from different scenarios or materials. If you check out Figure 4, you'll notice that the most stress shows up around the bolt holes and ribs. That's where the structure is working the hardest, mostly because of how it's supported and how the forces move through the shell. Everywhere else, the stress is much more even and drops off the farther you get from those busy areas. Figure 5 gives you a look at how the structure actually moves when pressure is applied. The areas that shift the most are those farthest away from where the enclosure is anchored, especially in the lower parts that take on more of the load. Closer to the bolt connections, movement is limited. This matches up perfectly with what we'd expect, given the way we set up the supports and loading in our model.

V. Discussion

The consistent, linear response we saw in the enclosure isn't just a basic feature of the material—it actually comes from the smart combination of the enclosure's shape, how it's held in place, and where the load is applied. What's really notable is that switching from a solid material to an infill-based one didn't cause any big changes in how the structure behaved. This shows that the design is robust: the overall performance stays steady, even when you tweak the material stiffness a bit. That's a real win for anyone focused on practical, design-oriented engineering. Here, using the effective Young's modulus from the RVE model helps us get a realistic picture of the structure's stiffness. If you use less infill, the material becomes less stiff, and not surprisingly, the part flexes a bit more. But importantly, the places where stress builds up and the overall pattern of movement don't really change. This lines up with what we expect: changing stiffness changes how much something bends, but the stress pattern itself is more about the loading and the design.

For designers, that's great news, it means you can use less infill to make lighter, quicker, and cheaper parts without raising the most critical stresses, as long as the extra flex is still okay for how the part will be used. This is especially useful for 3D-printed enclosures where keeping costs and print times down really matters.

By using effective properties instead of modeling every detail of the infill, our method lets you capture the key effects of the part's internal structure without making things overly complex. This not only makes the analysis much faster, but also lets you quickly try out changes to pressure, wall thickness, or geometry—no heavy-duty calculations required. This kind of flexibility is exactly what you want in the early design stages, when you need to spot problem areas and compare lots of different ideas without slowing down.

VI. Conclusion

In this study, the structural behavior of a printed ASA enclosure under external pressure was investigated using finite element analysis. In order to account for the infill effect without increasing the complexity of the model, the effective Young's modulus extracted from an RVE model was used and the resulting structural response was compared with the bulk material case. The results showed that in the range of pressures considered, the use of effective properties leads to a predictable increase in the displacement of the structure, while the critical stress level and stress distribution pattern are not affected.

This allows the use of less infill as a design tool to reduce the time and cost of construction, without increasing the critical stress in the structure. The presented approach can be used as a practical framework for the initial evaluation of printed enclosures under uniform external pressure and to support design decisions in the early stages of product design. Future work can focus on further improving and extending the presented framework. Experimental tests may be conducted to validate the numerical predictions and evaluate the behavior of printed enclosures under real operating conditions. In addition, the approach can be applied to different geometries, infill configurations and material systems to examine its general applicability. The influence of nonlinear effects, long-term loading and environmental factors such as temperature and moisture can also be explored to provide a more comprehensive understanding of the structural performance of additively manufactured enclosures under external pressure.

REFERENCES

[1] D. Bri, M. Garcia, J. Lloret, and P. Dini, “Real deployments of wireless sensor networks,” in Proc. Third Int. Conf. on Sensor Technologies and Applications (SENSORCOMM), Athens, Greece, June 2009, pp. 18–23.

[2] L. Parra, G. Lloret, J. Lloret, and M. Rodilla, “Physical sensors for precision aquaculture: A review,” IEEE Sensors Journal, vol. 18, no. 10, pp. 3915–3923, 2018.

[3] S.-H. Ahn, M. Montero, D. Odell, S. Roundy, and P. K. Wright, “Anisotropic material properties of fused deposition modeling ABS,” Rapid Prototyping Journal, vol. 8, no. 4, pp. 248–257, 2002.

[4] M. Domingo-Espín, J. M. Puigoriol-Forcada, A. A. Garcia-Granada, J. Llumà, S. Borros, and G. Reyes, “Mechanical property characterization and simulation of fused deposition modeling Polycarbonate parts,” Materials & Design, vol. 83, pp. 670–677, 2015.

[5] J. F. Rodríguez, J. P. Thomas, and J. E. Renaud, “Mechanical behavior of polymeric materials fabricated by fused deposition modeling,” Materials, vol. 11, no. 8, p. 1333, 2018.

[6] W. Cahyadi, Mechanical Properties of 3D Printed Acrylonitrile Styrene Acrylate (ASA), M.Sc. thesis, South Dakota State University, Brookings, SD, USA, 2019.

[7] Y. L. Yap, W. Y. Yeong, and Z. Y. Li, “Finite element analysis and ultrasonic characterization of 3D-printed ASA components,” Additive Manufacturing, vol. 28, pp. 363–371, 2019.

[8] A. Z. Hameed, S. Aravind Raj, J. Kandasamy, and M. A. Shahzad, “Optimization of 3D printing parameters for ASA using the Taguchi method,” Polymers, vol. 14, no. 16, p. 3256, 2022.

[9] J. M. Vázquez-Martínez, J. A. Pérez-Muñoz, and M. A. Camacho, “Evaluation of printing strategies on the mechanical and tribological response of ASA materials,” Rapid Prototyping Journal, vol. 27, no. 6, pp. 1035–1047, 2021.

[10] J. M. Chacón, M. A. Caminero, E. García-Plaza, and P. J. Núñez, “Additive manufacturing of PLA structures using fused deposition modelling: Effect of process parameters on mechanical properties,” Measurement, vol. 107, pp. 28–38, 2017.

[11] J. Torres, M. A. Cole, A. Owji, Z. DeMastry, and A. P. Gordon, “Effect of infill parameters on tensile mechanical behavior of FDM parts,” Procedia Manufacturing, vol. 1, pp. 211–218, 2015.

[12] B. Rankouhi, S. Javadpour, F. Delfanian, and T. Letcher, “Failure analysis and mechanical characterization of 3D printed ABS parts,” Materials & Design, vol. 108, pp. 609–622, 2016.

[13] A. R. Torrado and D. A. Roberson, “Failure analysis and anisotropy evaluation of 3D-printed polymers,” Engineering Failure Analysis, vol. 60, pp. 21–34, 2016.

[14] L. J. Gibson and M. F. Ashby, Cellular Solids: Structure and Properties, 2nd ed. Cambridge, U.K.: Cambridge University Press, 1997.

[15] Y. Zhang, J. Liu, and H. Yan, “Homogenization-based modeling of mechanical behavior of infill structures in additive manufacturing,” Composite Structures, vol. 184, pp. 831–839, 2018.

[16] T. J. Coogan and D. O. Kazmer, “Mechanical modeling of FDM materials considering interlayer bonding,” Additive Manufacturing, vol. 17, pp. 1–11, 2017.

[17] M. Somireddy, A. Czekanski, and S. Singh, “Effective mechanical properties of fused deposition modeling parts obtained through mesoscale modeling,” Additive Manufacturing, vol. 27, pp. 550–562, 2019.